

**Repository of the Max Delbrück Center for Molecular Medicine (MDC)
in the Helmholtz Association**

<https://edoc.mdc-berlin.de/21119/>

**A novel complex genomic rearrangement affecting the KCNJ2
regulatory region causes a variant of Cooks syndrome**

Cinque L., Micale L., Manara E., Esposito A., Palumbo O., Chiariello A.M., Bianco S., Guerri G., Bertelli M., Giuffrida M.G., Bernardini L., Notarangelo A., Nicodemi M., Castori M.

This is the final version of the accepted manuscript. The original article has been published in final edited form in:

Human Genetics
2022 FEB ; 141(2): 217-227
2021 NOV 25 (first published online: final publication)
Doi: [10.1007/s00439-021-02403-y](https://doi.org/10.1007/s00439-021-02403-y)

Publisher: [Springer Verlag](https://www.springer.com)

Copyright © The Author(s), under exclusive licence to Springer-Verlag GmbH Germany, part of Springer Nature 2021

Publisher's notice

This is a post-peer-review, pre-copyedit version of an article published in *Human Genetics*. The final authenticated version is available online at <https://doi.org/10.1007/s00439-021-02403-y>.

A novel complex genomic rearrangement affecting the *KCNJ2* regulatory region causes a variant of Cooks syndrome

Luigia Cinque,^{1*} Lucia Micale,^{1*} Elena Manara,² Andrea Esposito,³ Orazio Palumbo,¹ Andrea Maria Chiariello,³ Simona Bianco,⁴ Giulia Guerri,⁵ Matteo Bertelli,^{2,5,6} Maria Grazia Giuffrida,¹ Laura Bernardini,¹ Angelantonio Notarangelo,¹ Mario Nicodemi,^{3,4,7} and Marco Castori¹

1: Division of Medical Genetics, Fondazione IRCCS-Casa Sollievo della Sofferenza, Viale Cappuccini 1, 71013 San Giovanni Rotondo (Foggia), Italy. 2: MAGI Euregio, San Felice del Benaco (Brescia), Italy. 3: Dipartimento di Fisica, Università degli Studi di Napoli Federico II, and INFN Napoli, Complesso Universitario di Monte Sant'Angelo, Naples, Italy. 4: Berlin Institute for Medical Systems Biology, Max-Delbrück Centre (MDC) for Molecular Medicine, Berlin, Germany. 5: EBTNA-LAB, San Felice del Benaco (Brescia), Italy. 6: MAGI's Laboratory, Rovereto (Trento), Italy. 7: Berlin Institute of Health (BIH), MDC-Berlin, Germany. * these authors equally contributed to this work.

Declarations

Funding: this study was funded by the Italian Ministry of Health Ricerca Corrente 2018-2021.

Conflict of Interest: the authors declare no conflict of interest for this paper.

Ethics approval: this study was approved by the local Ethics Committee (protocol no. 13/CE/2021).

Consent to participate: the patient provided written informed consent for participation in this study.

Consent for publication: the patient signed a written informed consent for publication of molecular, clinical data and photographs.

Acknowledgments: The authors thank the family for their kind availability in sharing the findings within the scientific community.

Correspondence to:

Marco Castori, MD, PhD, Head

Division of Medical Genetics

Fondazione IRCCS-Casa Sollievo della Sofferenza

Viale Cappuccini 1

71013 San Giovanni Rotondo (Foggia)

Italy

Phone: +39 0882 416290

Email: m.castori@operapadrepio.it

Abstract

Cooks syndrome (CS) is an ultrarare limb malformation due to *in tandem* microduplications involving *KCNJ2* and extending to the 5' regulatory element of *SOX9*. To date, six CS families were resolved at the molecular level. Subsequent studies explored the evolutionary and pathological complexities of the *SOX9-KCNJ2/Sox9-Kcnj2* locus, and suggested a key role for the formation of novel topologically associating domain (TAD) by inter-TAD duplications in causing CS. Here, we report a unique case of CS associated with a *de novo* 1;17 translocation affecting the *KCNJ2* locus. On chromosome 17, the breakpoint mapped between *KCNJ16* and *KCNJ2*, and combined with a ~5 Kb deletion in the 5' of *KCNJ2*. Based on available capture Hi-C data, the breakpoint on chromosome 17 separated *KCNJ2* from a putative enhancer. Gene expression analysis demonstrated downregulation of *KCNJ2* in both patient's blood cells and cultured skin fibroblast. Our findings suggest that a complex rearrangement falling in the 5' of *KCNJ2* may mimic the developmental consequences of *in tandem* duplications affecting the *SOX9-KCNJ2/Sox9-Kcnj2* locus. This finding adds weight to the notion of an intricate role of gene regulatory regions and, presumably, the related three-dimensional chromatin structure in normal and abnormal human morphology.

Key words: brachydactyly, Cooks syndrome, deletion, *KCNJ2*, TAD, *SOX9*

Introduction

Recent advances indicate that a better understanding of the mechanisms which regulate the three-dimensional (3D) organization of chromatin is crucial for a far-reaching knowledge of health and disease in humans. Chromatin interactions tend to occur within defined and stable genomic regions, usually defined as topologically associating domains (TADs) (Dixon et al., 2012; Rao et al., 2014). TADs are genomic domains corresponding to chromatin loops which trace the blueprint for the enhancer-promoter interactions in regulating gene expression. Adjacent TADs are separated by DNA sequences which are the targets of insulator proteins, such as CTCF (Ibrahim et al., 2020). In selected and still incompletely understood circumstances, genomic structural variations disrupting, duplicating, deleting and/or reshuffling TADs are sufficient for determining developmental disorders (Lupiáñez et al., 2016). This presumably occurs due to a change of the regulatory landscape in which the enhancer elements interact with ectopic promoters and this causes gene misexpression (Franke et al., 2016). In the near future, technologies specifically addressed for the study of the 3D chromatin organization promise an improvement of the diagnostic yield of laboratory workflows in developmental disorders (Melo et al., 2020).

Cooks syndrome (CS) is a variant of brachydactyly type B, characterized by nail hypo/aplasia, hypoplastic nail tufts and elongation of the distal phalanges; some digits may have only two phalanges (Mundlos and Horn, 2014). In 2009, four families with CS were described with similar microduplications with a minimum region of overlap of ~1.2 Mb encompassing the 5' regulatory regions of *SOX9* and including *KCNJ2* (Kurth et al., 2009). Two additional families were subsequently described with overlapping duplications (Liu et al., 2020; Melo et al., 2020). *SOX9* encodes for a transcription factor that plays a key role in chondrocytes differentiation and skeletal development (Haseeb et al., 2021). Heterozygous, *loss-of-function* variants of *SOX9* typically cause campomelic dysplasia, which is a severe skeletal dysplasia with or without sex-reversal in XY individuals and Robin sequence, and its milder variant acampomelic dysplasia. In addition to CS, copy number variations (CNV) involving the 5' regulatory region of *SOX9* are associated with a wider spectrum of clinical manifestations ranging from lethal campomelic dysplasia with sex reversal and Robin sequence, to acampomelic dysplasia, to developmental restricted phenotypes including isolated sex-reversal/gonadal dysgenesis and Robin sequence (Castori et al., 2016).

KCNJ2 maps at the 5' of *SOX9* and encodes for an integral membrane protein and inward-rectifier type potassium channel which likely participates to establish action potential waveform and excitability of neuronal and muscle tissues. Single nucleotide deleterious variants of *KCNJ2* and, more rarely, large deletions encompassing the gene have been associated with Andersen-Tawil syndrome, characterized by the triad of periodic paralysis, cardiac arrhythmias, and facial and minor skeletal anomalies (Jeong et al., 2020).

In mouse, *Sox9* is markedly expressed in the distal mesenchymal condensations and, subsequently, in the developing terminal phalanges and claws, a fact suggesting a key role for *SOX9* dysregulation in

the etiopathogenesis of CS (Kurth et al., 2009). Further studies demonstrated that an *in tandem* duplication in mouse, selectively incorporating the *Sox9* 5' regulatory element and *Kcnj2*, generates a neo-TAD in which *Kcnj2* ectopically interacts with the adjacent *Sox9* regulatory region and, then, is misexpressed (Franke et al., 2016). Mouse modelling experiments showed that specific inversions fusing the *Sox9* and *Kcnj2* TADs associate with a malformed digit phenotype resembling CS and featuring *Kcnj2* misexpression in a *Sox9*-like pattern during terminal limb development (Despang et al., 2019). These findings in mice suggest complex mechanisms underlying genotype-phenotype correlations in CNVs affecting the *SOX9-KCNJ2* regulatory region.

We report a novel patient with a variant of CS sparing I digits and caused by a *de novo* 1;17 translocation affecting the *SOX9-KCNJ2* locus. On chromosome 17, the breakpoint mapped at the 5' of *KCNJ2* and generated a ~5 Kb microdeletion involving the *KCNJ2* upstream region. Our observation broadens the spectrum of the genomic rearrangements causing CS.

Materials and Methods

Patient enrollment

The patient and her parents were originally enrolled during the routine clinical activity of the Division of Medical Genetics at Fondazione IRCCS-Casa Sollievo della Sofferenza, San Giovanni Rotondo (Italy). The family provided signed informed consent to undergo blood sampling for the following investigations. The patient also underwent skin biopsy for cell culture and signed a written informed consent for publication of molecular, clinical data and photographs. This study was conducted in accordance with the 1984 Helsinki declaration and its following modifications and was approved by the local Ethics Committee (protocol no. 13/CE). Fibroblast cultures were deposited into Genomic and Genetic Disorders Biobank at the Fondazione IRCCS-Casa Sollievo della Sofferenza, San Giovanni Rotondo, Italy (protocol no. GTB12001).

Conventional cytogenetic analysis and fluorescence in situ hybridization (FISH)

Peripheral blood was collected and metaphase chromosome preparations were obtained from phytohemagglutinin-stimulated lymphocyte cultures according to standard procedures (Silva et al, 2018). Routine cytogenetic analysis by G-banding techniques at the 550 bands of resolution was performed. Metaphases were examined under a Leica DM2500 (Leica, Wetzlar, Germany) microscope using 20X and 100X objective lenses. Locus-specific fluorescence *in situ* hybridization (FISH) was performed to verify translocation breakpoints. The FISH probes were set up using bacterial artificial chromosome (BAC) clones belonging to the 32K library (<https://bacpacresources.org/genomicRearrays.php>), whose mapping data was derived from public databases (<http://dgv.tcag.ca/dgv/app/home>; Clones on SMRT BAC Array Track, hg19 Release). DNA was extracted by Quantum Prep MiniPrep Kit (BioRad, Hercules, CA) and was labeled with SpectrumGreen-dUTP or SpectrumOrange-dUTP by using the Nick Translation kit (Abbott Laboratories, Abbott Park, IL) according to the manufacturer's protocol. FISH analysis was performed

on chromosome spread using probes: RP11-633A13 (green), N0693H11 (orange) and RP11-727K24 (orange) specific for 17q24.3 region while RP11-706N07 (green) and RP11-147B11 (green) specific for 1p32.1 and 1p32.2 regions, respectively. FISH was performed by co-denaturing probes and chromosomes at 74 °C for 3 min, and keeping the slides into the hybridisation chamber (Hybrite; Abbott Laboratories, Abbott Park, IL) at 37 °C overnight. After three washes, metaphases were counterstained with 4',6-diamidin-2-fenilindol (DAPI) (Leica, Wetzlar, Germany).

Chromosome microarray analysis (CMA)

Genomic DNA was extracted from patients' and unaffected relatives' peripheral blood leucocytes by using Bio Robot EZ1 and QIAamp DNA Mini Kit (Qiagen, Tübingen, Germany) according to the manufacturer's instructions. The DNA was quantified with Qubit spectrophotometer (ThermoFisher Scientific, Wilmington DE, USA). CMA on patient's DNA was carried out by using the CytoScan HD array (ThermoFisher Scientific, Wilmington DE, USA) as previously described (Palumbo et al., 2014). Data analysis was performed using the Chromosome Analysis Suite Software version 4.2 (ThermoFisher Scientific, Wilmington DE, USA) following a standardized pipeline (Palumbo et al., 2020). Briefly: (i) the raw data file (.CEL) was normalized using the default options; (ii) an unpaired analysis was performed using 270 HapMap samples as a baseline in order to obtain copy numbers value from .CEL files. The amplified and/or deleted regions were detected using a standard Hidden Markov Model (HMM) method. As this investigation was carried out in order to refine a previously known structural rearrangement (see "Results"), we retained CNVs ≥ 1 Kb in length and overlapping ≥ 10 consecutive probes to reduce the detection of false-positive calls. The significance of each CNV detected was determined by comparison with all chromosomal alterations identified in the patient to those collected in an internal database of ~4500 patients studied by SNP arrays since 2010, and public databases including database of genomic variants (DGV; <http://projects.tcag.ca/variation/>), database of genomic variation and phenotype in humans using Ensembl resources (DECIPHER; <https://decipher.sanger.ac.uk/>), and ClinVar (<https://www.ncbi.nlm.nih.gov/clinvar/>). Base pair positions, information about genomic regions and genes or functional elements affected by CNVs, and known associated diseases have been derived from the University of California Santa Cruz (UCSC) Genome Browser, build GRCh38 (hg38). The clinical significance of each rearrangement detected was assessed following the American College of Medical Genetics (ACMG) guidelines (Riggs et al., 2020). This analysis was repeated twice for internal confirmation on patient's DNA and carried out on both parents' DNA for segregation analysis.

Genome sequencing (GS)

The DNA from the patient was prepared according to the Illumina Truseq PCR free library prep protocol and measured by PicoGreen and Nanodrop (ThermoFisher Scientific, Wilmington DE, USA). Briefly, one microgram of genomic DNA for a 350bp insert size was fragmented by covaris. The fragmented DNA was blunt-ended and phosphorylated, following end repair, the appropriate library size was

selected using different ratios of the sample purification beads. A single 'A' was ligated to the 3' end, Illumina adapters was then ligated to the fragments. The final ligated product was quantified using quantitative PCR (qPCR) according to the qPCR Quantification Protocol Guide and qualified using the Agilent Technologies 2100 Bioanalyzer. (Agilent Technologies, Palo Alto CA, USA). Then, a 150 bp paired-end read sequencing was performed using the NovaSeq™ 6000 platform (Illumina, San Diego CA, USA) according to the manufacturer's instructions.

The quality of the Illumina raw reads was assessed with the FASTQC software, then low quality bases and adapter sequences were removed with the software Trimmomatic (<http://www.usadellab.org/cms/?page=trimmomatic>) (minimum Phred quality 35 and minimum length 50 bp). The quality of the trimmed files was checked again with FASTQC. The samples had 2,593,097,392 raw reads and 2,590,253,116 trimmed reads. The high quality reads were mapped against the human reference genome (hg38, downloaded from the Ensembl Database) using the minimap2 software (<https://github.com/lh3/minimap2>). The file was then sorted and optical duplicates were removed with Picard (<https://broadinstitute.github.io/picard/>). The obtained mapping file was used to detect the presence of structural variants using the Manta algorithm (<https://github.com/Illumina/manta/>). The .VCF files were annotated with VEP. The raw variant files were filtered to retain only the ones classified as PASS and with a coverage of at least 10 reads. The average mapping rate of all samples was approximately 99.5% and the average sequencing genome coverage was 100×. Genome sequencing and data analysis was carried out by Sequentia Biotech (Barcelona, Spain). PCR primers were designed on either side of the two potential breakpoint regions on the derivative versions of chromosomes 1 and 17 identified by GS. DNA sequencing was performed by PCR using a AmpliTaq Gold™ 360 PCR Master Mix (Applied Biosystem, Vilnius, Lithuania) according to the manufacturer's specifications, confirmed by bidirectional Sanger sequencing on a CEQ8800 Sequencer (Beckman Coulter, Fullerton, CA, USA).

Hi-C data and regulatory elements analysis

To study the three-dimensional organization of the genomic regions around the breakpoints, we employed published Hi-C data, which provide genome-wide chromatin interaction frequencies between genomic loci using crosslinking and proximity ligation (Lieberman-Aiden et al., 2009, Kempfer and Pombo, 2019). In particular, we considered two genomic regions (chr17:67700000-72700000 and chr1:57900000-62900000, hg38) centered around the breakpoints of the translocation. Hi-C data of these regions in IMR90 were taken from Rao et al., 2014 and were shown at 10kb resolution. Coordinates were mapped using UCSC Genome Browser LiftOver tool. To investigate the potential impact on gene regulation caused by the rearrangement of the regulatory elements following the translocation, we downloaded the position of putative enhancers in IMR90 from the ENCODE Registry of Candidate cis-Regulatory Elements (ENCODE Project Consortium et al., 2020). Briefly, in this database putative enhancers are defined as regions enriched in both DNase and histone 3 lysine 27 acetylation (H3K27ac) in IMR90 cell line. As additional control, we used normalized promoter capture

Hi-C data, a variant of HiC useful to annotate candidate target genes for cis-regulatory elements (Jung et al., 2019). Specifically, we considered a genomic region extending 2Mb downstream and upstream *KCNJ2* and *SOX9* promoters. Interaction values with a p-value < 0.01 were taken as significant.

Fibroblasts cell culture

Primary dermal fibroblasts were established from skin biopsies of patient and healthy controls and cultured in Dulbecco's-Modified Eagle Medium/Nutrient Mixture F-12 (D-MEMF12) (ThermoFisher Scientific, Wilmington DE, USA), plus 10% fetal bovine serum (FBS) (ThermoFisher Scientific, Wilmington DE, USA) and 1% streptomycin and penicillin (ThermoFisher Scientific, Wilmington DE, USA), as previously described (Morlino et al., 2019) and grown in a 5% CO₂ incubator at 37° C. The controls included seven females and only one male; the mean age of all individuals was 25 years, with a range from 5 years to 45 years.

Sample processing, RNA extraction and cDNA synthesis

Total RNA was extracted from peripheral blood of proband and healthy control samples, using PAXgene Blood RNA kit (Qiagen, Tübingen, Germany) according to the manufacturer's protocol. The control cohort included seven females and one male; the mean age of all individuals was 26 years, with a range from 22 years to 34 years. Total RNA was extracted from cultured skin fibroblasts with the RNeasy Mini Kit (Qiagen, Tübingen, Germany). RNAs were treated with RNase free-DNase (Qiagen, Tübingen, Germany), quantified by Nanodrop (Thermo Fisher Scientific, Waltham, Massachusetts, USA), and reverse-transcribed with the QuantiTect Reverse Transcription Kit (Qiagen, Tübingen, Germany), according to the manufacturer's protocol.

Gene expression analysis

RNAs extracted were processed for qPCR to measure *SOX9* and *KCNJ2* mRNA expression levels in patient's peripheral blood (*KCNJ2*) and fibroblasts (*SOX9* and *KCNJ2*), as well as in eight healthy control samples. The transcriptional levels of some genes located in the proximity of the genomic rearrangement (*KCNJ16*, *SLC39A11*, *FGGY* and *DOCK7*) and an unrelated gene (*TAB2*) were qPCR profiled in both patient's and control's blood cells and cultured skin fibroblasts in order to verify the specificity of *SOX9* and *KCNJ2* expression. These genes were selected on the basis of their expression in both analyzed tissues. Oligos for quantitative PCR were designed using the Primer express program (Rozen and Skaletsky, 2000) with default parameters (**Table S1**). Primers were blasted against human genome by BLAST to ensure specificity. Glyceraldehyde phosphate dehydrogenase (GAPDH) and 18S ribosomal RNA were used as reference genes. The reactions were run in triplicate in 10 µl of final volume with 10 ng of sample complementary DNA (cDNA), 0.3mM of each primer, and 1× Power SYBR Green PCR Master Mix (ThermoFisher Scientific, Wilmington DE, USA). Reactions were set up in a 384-well plate format (ThermoFisher Scientific, Wilmington DE, USA) and run in an ABI Prism 7900HT (ThermoFisher Scientific, Wilmington DE, USA) with default amplification conditions. Raw Ct values were obtained using SDS 2.3 (Applied Biosystem, Vilnius, Lithuania). Calculations were

carried out by the comparative Ct method as reported in Micale et al. (2014). Significance was determined by an unpaired, two-sample t-tests.

Results

Clinical report

The patient was an 18-year-old woman who requested Clinical Genetics consultation because “she was born without nails”. Shortly after birth, she underwent standard karyotyping which revealed a *de novo* 1;17 reciprocal translocation, but, at that time, this finding was not related to the developmental abnormality. The patient was otherwise healthy. She regularly reached developmental milestones and had a satisfactory education. At 6 years, she developed myopia which was -6 diopters in both eyes at last ophthalmological examination. At 17 years, she was diagnosed with coeliac disease. At examination, fingers II to V lacked nails and had a bulbous tip, particularly on fingers II-IV. Fingers V appeared shortened compared to the others (**Fig. 1a**). Thumbs were normal with intact nails. Fingers were also hyperextensible at the proximal and distal interphalangeal joints. On feet, toes II-V did not have nails and were shortened with a bulbous tip, while the big toes looked normal (**Fig. 1b**). There was not any facial dysmorphism. Plain radiographs showed two phalanges in fingers V (either missing middle phalanx, or missing distal phalanx with a middle phalanx with a distal-like shape) and hypoplastic ungual tufts (**Fig. 1c**). On toes II-V, only two phalanges were visible with distal elongation and hypoplastic ungual tufts (**Fig. 1d**). Full cardiologic examination ruled out any heart structural and rhythm anomalies.

Cytogenetic and cytogenomic analysis

One hundred metaphases from cultured lymphocytes were examined in the proband and her parents. A reciprocal translocation between the short arm of chromosome 1 and long arm of chromosome 17 at bands 1p32.1 and 17q24.3 was identified in the proband but not in the parents (**Fig. 1e**). FISH analysis was able to confirm the breakpoints in 17q24.3 in the *SOX9* 5' region and in close proximity to *KCNJ16* and *KCNJ2*, and in a gene desert region mapping in 1p32.1 (**Fig. 1f-l**). CMA revealed that the reciprocal translocation is unbalanced due to concurring interstitial microdeletions involving the 17q24.3 and the 1p32.1 chromosome regions. In detail, the deleted region on chromosome 17 was at least 5 Kb in size and covered by 14 SNP array probes (from C-3HNQV to C-5XLTR) while the deleted region on chromosome 1 was at least 3 Kb in size and covered by 7 SNP array probes (from C_4LHXN to C_5CRVZ) (**Fig. 2a; Fig. S1**). No additional clinically significant copy number changes were identified. Carrier testing in the parents proved a *de novo* origin of both microdeletions in the patient. The molecular karyotype of the patient, according with the International System for Human Cytogenetic Nomenclature (ISCN 2020), was: arr[GRCh38] 17q24.3(70158324_70162696)x1 dn and arr[GRCh38] 1p32.1(60319779_60322850)x1 dn. Both microdeletions involved gene desert regions. The microdeletion affecting the 17q24.3 sub-band fell within the *SOX9-KCNJ2* regulatory region. The distal (telomeric) breakpoint of the CNV on 17q24.3 was located between *KCNJ16* and *KCNJ2* and, more

specifically, ~6 Kb away from the 5' region of *KCNJ2* and ~1.9 Kb from the 3' region of *KCNJ16* (**Fig. 2a**).

Breakpoint refinement by GS

The aim of the experiment was to detect translocations between chromosomes 1 and 17. Translocations between chromosomes 1 and 17 highlighted by GS sequencing and that confirmed FISH analysis results are showed in **Table S2**. All the variants were heterozygous. The t(1;17)(p32.1;q24.3) reciprocal translocation junction fragment was amplified using both primer pairs in all family members. Amplification was visible just in the proband confirming a *de novo* origin. The breakpoint on the derivative chromosome 1 had a sequence microhomology of 14 bp (TGAGGAATCGCCAC). The last unique base of chromosome 1p was at 60323941 (hg38) and the first unique base of chromosome 17q was at 70163514 (hg38) (**Fig. 2b**). The breakpoint on the derivative chromosome 17 had a sequence overlap of 3 bp (TAC) and the last unique base of chromosome 1p was at 60318669 (hg38) and the first unique base of chromosome 17q was at 70158349 (hg38) (**Fig. 2b**). This resulted in a deletion of 5272 bp on chromosome 1 and of 5151 bp on chromosome 17 (**Fig. 2c**).

Analysis of Hi-C data and expression study

Fig. 3a, b shows the regulatory landscape around the translocation breakpoints. Hi-C contact matrices reveal that the breakpoint on chr17 falls in the middle of the *KCNJ2* TAD (Franke et al., 2016), at the boundary between two sub-domains (**Fig. 3a**) and the breakpoint on chr1 is located within a larger TAD, in a gene desert region (**Fig. 3b**). The region proximal to the breakpoint on chr17 contains several IMR90 putative enhancers, whereas they are absent around the breakpoint on chr1. Furthermore, promoter capture Hi-C data showed that *KCNJ2* promoter tends to form significant interactions with putative regulatory elements upstream the breakpoint (bottom part of **Fig. 3a**). As a result of the translocation, such putative enhancers are moved away from *KCNJ2*. Taken together, these observations suggested a potential alteration in the regulatory conditions of *KCNJ2*. Therefore, in order to evaluate the functional impact of the t(1;17)(p32.1;q24.3) reciprocal translocation at the *KCNJ2* transcriptional level, we quantified the *KCNJ2* mRNA expression in the patient's fibroblasts and lymphocytes, compared to healthy control fibroblasts and lymphocytes, respectively. qPCR analysis revealed a decrease (50%) of *KCNJ2* expression level in both analyzed blood cells and cultured skin fibroblasts, compared to the controls (**Fig. 3c, d**). We also monitored a downregulation of *SOX9* mRNA amount (40%) in the patient fibroblasts, respect to controls (**Fig. 3e**). We were not able to test *SOX9* levels in blood because it is not physiologically expressed in this tissue. To demonstrate the specificity of *KCNJ2* and *SOX9* downregulation in patient's tissues, we qPCR-profiled some genes mapping in the proximity of the genomic rearrangement on chromosome 17 (*KCNJ16* and *SLC39A11*) and chromosome 1 (*FGGY* and *DOCK7*), as well as on an unrelated locus (*TAB2*). *KCNJ16* expression levels were undetectable in both analysed tissues as a consequence of its low or absent expression. Conversely, quantitative analysis detected that *SLC39A11*, *FGGY*, *DOCK7*, and *TAB2* transcriptional

levels were comparable between patient's and healthy control fibroblast and lymphocytes. These data support the specificity of *KCNJ2* and *SOX9* downregulation in patient's tissues compared to controls (Fig. S2).

Discussion

The pathogenic role of most CNVs can be explained by their effect on dosage-sensitive genes. In contrast, clinical interpretation of structural variations affecting gene-desert or regulatory regions remains complicated. Such variants have the potential to disrupt the integrity of the genome by causing changes in the regulatory architecture that lead to alterations of gene expression levels and patterns (Haraksingh and Snyder, 2013; Spielmann and Mundlos, 2013). However, the lack of a comprehensive understanding of the large-scale functional organization of the regulatory genome is a major limitation in predicting their potential pathogenicity. Genome-wide interaction studies by chromosome conformation capture based approaches, such as Hi-C (a high-throughput variant of the chromosome conformation capture technique) and chromosome conformation capture carbon copy technologies, are helping medical research in dissecting the potential mechanisms underlying the postulated pathological effect in candidate genomic disorders. Thanks to these novel approaches, the number of developmental disorders that are consistently associated with rearrangements affecting non-coding regions is increasing. Genomic disorders involving the *SOX9-KCNJ2* genomic region are a prototype for the complexities underlying normal and abnormal variability related to CNVs which involve regulatory regions.

Here, we reported the first patient with a variant of CS and a *de novo* translocation disrupting the *KCNJ2* locus. To the best of our knowledge, only six families were previously described with CS and partially overlapping duplications involving the 5' regulatory region of *SOX9* and the proximally placed *KCNJ2* (Kurth et al., 2009; Liu et al., 2020; Melo et al., 2020). The present patient showed a *de novo* 1;17 unbalanced translocation with breakpoints falling between *KCNJ16* and *KCNJ2*, and associating with a ~5 Kb microdeletion in the 5' of *KCNJ2*. The latter caused the loss of predicted enhancer and promoter sequences of *KCNJ2*. The impact of this rearrangement at the gene transcriptional level was explored by mRNA analysis, which showed reduced transcription of *KCNJ2* and *SOX9* in cultured fibroblasts. We also monitored a *KCNJ2* expression reduction in patient's peripheral lymphocytes compared to controls with similar results. *SOX9* was not tested because it is not physiologically expressed in blood. The *SOX9-KCNJ2/Sox9-Kcnj2* locus structure was finely studied. Hi-C shows a compartmentalization of the human locus in two major TADs, one containing *SOX9* and the other containing the two potassium channel *KCNJ2* and *KCNJ16* (Dixon, et al., 2012). The large gene desert corresponding to the *SOX9* TAD was shown to contain multiple regulatory elements and human-disease-related sites (Gordon et al., 2009). Mouse experiments demonstrated that intra-TAD duplications selectively involving *Kcnj16* and *Kcnj2* and thus simply introducing an extra dose of *Kcnj2* did not result in any abnormal phenotype. Conversely, a CS-like condition was observed in mice carrying an inter-TAD

duplication involving *Kcnj2* but also extending over the 5' regulatory region of *Sox9* (Franke et al., 2016). This prompted the authors to speculate that the dosage-sensitivity of genes involved in specific developmental disorders can manifest in an abnormal outcome only when these genes are included in neo-TADs generated by inter-TAD duplications (Franke et al., 2016). This concept was further supported by additional experiments which showed severely dysplastic nails in mice carrying an inversion fusing the inverted centromeric *Sox9* TAD with the *Kcnj2* TAD (Despang et al., 2019). In these mice, *Sox9* was downregulated by 20% and *Kcnj2* was overexpressed by 50%. Whole-mount *in situ* hybridization in E12.5 mice embryos clearly demonstrated a *Sox9*-like pattern of misexpression for *Kcnj2* in the appendicular anlagen (Despang et al., 2019). More specifically, in CS mice embryos, the most striking finding was an overexpression of *Kcnj2* on appendicular bones in a pattern overlapping the tissue-specific physiological expression of *Sox9*, which is therefore less significantly affected by inter-TAD duplications or inversions (Franke et al., 2016; Despang et al., 2019).

In our patient, analysis of Hi-C around the two breakpoints on chromosomes 1 and 17 indicated that the breakpoint on chromosome 17 and the corresponding microdeletion mapped in a region enriched in IMR90 specific putative enhancers located in the middle of the *KCNJ2* TAD. The resulting translocation presumably put *KCNJ2* in a novel regulatory landscape. The *KCNJ2-SOX9* boundary, which is downstream to the rearrangement breakpoint on chromosome 17, has a strong insulator score. Therefore, it is unlikely, though not formally demonstrated in this work, that the 1;17 translocation would disturb this boundary. However, on the basis of the clinical similarities between our patient and the other CS individuals carrying the “more classic” microduplication, it is plausible, that in the former, *KCNJ2* and *SOX9* could have been influenced by different regulatory elements put on the centromeric sequences of chromosome 1, such as the TADs containing *C1orf87* and/or *CYP2J2*, during key stages of appendicular development. This could have led to a pattern of *KCNJ2* misexpression similar to that which is thought to be occurred during limb development of the previously published patients with CS and the ~1.2 Mb microduplication involving *KCNJ2*. In this context, the observed downregulation of *KCNJ2* in both skin fibroblasts and peripheral blood, and the downregulation of *SOX9* in skin fibroblasts of our patient can be interpreted as the disruptive effects on gene transcription of the novel rearrangements in the post-natal life.

The mechanisms explaining the downregulation of *KCNJ2* and *SOX9* expression in mature tissues, and its presumed relationship with the predicted *KCNJ2* misexpression during key stages of limb development remain obscure in this patient. Nevertheless, we could exclude that this rearrangement caused haploinsufficiency of *SOX9* and/or *KCNJ2* during *in utero* development on clinical grounds. In fact, haploinsufficiency of *SOX9* due to deletions involving its 5' regulatory region typically leads to a generalized skeletal phenotype (i.e. campomelic or acampomelic dysplasia) (Castori et al., 2016), which does not feature the CS-typical anonychia and was absent in this case. In addition, deletions of the entire *KCNJ2* gene is a rare cause of Andersen-Tawil syndrome (Marquis-Nicholson et al., 2014), whose pathognomonic features were not observed in our patient. The unique nature of the identified

rearrangement may reflect the minor clinical differences between our patient and those previously reported with the ~1.2 Mb microduplication involving *KCNJ2*. In particular, our patient showed sparing of I digits and this could have been determined by either minor difference in *KCNJ2* misexpression pattern during limb development or altered expression of interacting genes adjacent to the involved region on chromosome 1 or both.

In conclusion, our data indicate that CS can be caused by a wider spectrum of rearrangements involving the *KCNJ2* locus. The selective deletion of the *KCNJ2* putative enhancer region and the predicted disruption of the *KCNJ2* TAD by the translocation breakpoint reinforce the hypothesis that a *KCNJ2* misexpression during specific developmental stages is the key event in the pathogenesis of CS, as previously stated (Franke et al., 2016). Our observation adds observations that could stimulate further research aimed at exploring such a complex pathogenesis of CS.

References

Castori M, Bottillo I, Morlino S, Barone C, Cascone P; Pediatric Craniofacial Malformation (PECRAM) Study Group, Grammatico P, Laino L. Variability in a three-generation family with Pierre Robin sequence, acampomelic campomelic dysplasia, and intellectual disability due to a novel ~1 Mb deletion upstream of SOX9, and including KCNJ2 and KCNJ16. *Birth Defects Res A Clin Mol Teratol* 2016;106(1):61-8.doi: 10.1002/bdra.23463.

Castori M, Brancati F, Mingarelli R, Mundlos S, Dallapiccola B (2007) A novel patient with Cooks syndrome supports splitting from "classic" brachydactyly type B. *Am J Med Genet A* 143A(2):195-9.doi: 10.1002/ajmg.a.31433.Despang A, Schöpflin R, Franke M, Ali S, Jerković I, Paliou C, Chan WL, Timmermann B, Wittler L, Vingron M, Mundlos S, Ibrahim DM (2009) Functional dissection of the Sox9-Kcnj2 locus identifies nonessential and instructive roles of TAD architecture. *Nat Genet* 51(8):1263-71.doi: 10.1038/s41588-019-0466-z.

Dixon JR, Selvaraj S, Yue F, Kim A, Li Y, Shen Y, Hu M, Liu JS, Ren B (2012) Topological domains in mammalian genomes identified by analysis of chromatin interactions. *Nature* 485(7398):376-80. doi: 10.1038/nature11082.

ENCODE Project Consortium, Moore JE, Purcaro MJ, Pratt HE, Epstein CB, Shores N, Adrian J, Kawli T, Davis CA, Dobin A, Kaul R, Halow J, Van Nostrand EL, Freese P, Gorkin DU, Shen Y, He Y, Mackiewicz M, Pauli-Behn F, Williams BA, Mortazavi A, Keller CA, Zhang XO, Elhajjajy SI, Huey J, Dickel DE, Snetkova V, Wei X, Wang X, Rivera-Mulia JC, Rozowsky J, Zhang J, Chhetri SB, Zhang J, Victorsen A, White KP, Visel A, Yeo GW, Burge CB, Lécuyer E, Gilbert DM, Dekker J, Rinn J, Mendenhall EM, Ecker JR, Kellis M, Klein RJ, Noble WS, Kundaje A, Guigó R, Farnham PJ, Cherry JM, Myers RM, Ren B, Graveley BR, Gerstein MB, Pennacchio LA, Snyder MP, Bernstein BE, Wold B, Hardison RC, Gingeras TR, Stamatoyannopoulos JA, Weng Z (2020) Expanded encyclopaedias of DNA elements in the human and mouse genomes. *Nature* 583(7818):699-710. doi: 10.1038/s41586-020-2493-4.

Franke M, Ibrahim DM, Andrey G, Schwarzer W, Heinrich V, Schöpflin R, Kraft K, Kempfer R, Jerković I, Chan WL, Spielmann M, Timmermann B, Wittler L, Kurth I, Cambiaso P, Zuffardi O, Houge G, Lambie L, Brancati F, Pombo A, Vingron M, Spitz F, Mundlos S (2016) Formation of new chromatin domains determines pathogenicity of genomic duplications. *Nature* 538 (7624):265-9.doi: 10.1038/nature19800

Gordon CT, Tan TY, Benko S, Fitzpatrick D, Lyonnet S, Farlie PG (2009) Long-range regulation at the SOX9 locus in development and disease. *J Med Genet* 46(10):649-56. doi: 10.1136/jmg.2009.068361.

Haraksingh RR, Snyder MP. Impacts of variation in the human genome on gene regulation (2013) *J Mol Biol* 425(21):3970-7. doi: 10.1016/j.jmb.2013.07.015.

Haseeb A, Kc R, Angelozzi M, de Charleroy C, Rux D, Tower RJ, Yao L, Pellegrino da Silva R, Pacifici M, Qin L, Lefebvre V (2021) SOX9 keeps growth plates and articular cartilage healthy by inhibiting chondrocyte dedifferentiation/osteoblastic redifferentiation. *Proc Natl Acad Sci U S A*. 23;118(8):e2019152118. doi: 10.1073/pnas.2019152118.

Ibrahim DM, Mundlos S (2020) The role of 3D chromatin domains in gene regulation: a multi-faceted view on genome organization. *Curr Opin Genet Dev* 61:1-8. doi: 10.1016/j.gde.2020.02.015.

Kurth I, Klopocki E, Stricker S, van Oosterwijk J, Vanek S, Altmann J, Santos HG, van Harssel JJ, de Ravel T, Wilkie AO, Gal A, Mundlos S (2009) Duplications of noncoding elements 5' of SOX9 are associated with brachydactyly-anonychia. *Nat Genet* 41(8):862-3. doi: 10.1038/ng0809-862.

Jeong DU, Jiyeong Lee J, Lim KM (2020) Computational Study to Identify the Effects of the KCNJ2 E299V Mutation in Cardiac Pumping Capacity. *Comput Math Methods Med* (31): 7194275. doi: 10.1155/2020/7194275.

Jung I, Schmitt A, Diao Y, Lee AJ, Liu T, Yang D, Tan C, Eom J, Chan M, Chee S, Chiang Z, Kim C, Masliah E, Barr CL, Li B, Kuan S, Kim D, Ren B (2019) A compendium of promoter-centered long-range chromatin interactions in the human genome. *Nat Genet* 51(10):1442-1449. doi: 10.1038/s41588-019-0494-8.

Liu M, Zhang X, Liu H, Shen Y (2020) A 17q24.3 duplication identified in a large Chinese family with brachydactyly-anonychia. *Mol Genet Genomic Med*. doi: 10.1002/mgg3.1392.

Lupiáñez DG, Spielmann M, Mundlos S (2016) Breaking TADs: How Alterations of Chromatin Domains Result in Disease. *Trends Genet* 32(4):225-37. doi: 10.1016/j.tig.2016.01.003.

Marquis-Nicholson R, Prosser DO, Love JM, Zhang L, Hayes I, George AM, Crawford JR, Skinner JR, Love DR (2014) Array comparative genomic hybridization identifies a heterozygous deletion of the entire KCNJ2 gene as a cause of sudden cardiac death. *Circ Cardiovasc Genet* 7(1):17-22. doi: 10.1161/CIRCGENETICS.113.000415.

Melo US, Schöpflin R, Acuna-Hidalgo R, Mensah MA, Fischer-Zirnsak B, Holtgrewe M, Klever MK, Türkmen S, Heinrich V, Pluym ID, Matoso E, Bernardo de Sousa S, Louro P, Hülsemann W, Cohen M, Dufke A, Latos-Bieleńska A, Vingron M, Kalscheuer V, Quintero-Rivera F, Spielmann M, Mundlos S (2020) Hi-C Identifies Complex Genomic Rearrangements and TAD-Shuffling in Developmental Diseases. *Am J Hum Genet* 106(6):872-84. doi: 10.1016/j.ajhg.2020.04.016.

Micale L, Augello B, Maffeo C, Selicorni A, Zucchetti F, Fusco C, De Nittis P, Pellico MT, Mandriani B, Fischetto R, Boccone L, Silengo M, Biamino E, Perria C, Sotgiu S, Serra G, Lapi E, Neri M, Ferlini A, Cavaliere ML, Chiurazzi P, Monica MD, Scarano G, Faravelli F, Ferrari P, Mazzanti L, Pilotta A, Patricelli MG, Bedeschi MF, Benedicenti F, Prontera P, Toschi B, Salviati L, Melis D, Di Battista E, Vancini A, Garavelli L, Zelante L, Merla G (2014) Molecular analysis, pathogenic mechanisms, and

readthrough therapy on a large cohort of Kabuki syndrome patients. *Hum Mutat* 35(7):841-50. doi: 10.1002/humu.22547.

Morlino S, Carbone A, Ritelli M, Fusco C, Giambra V, Nardella G, Notarangelo A, Panelli P, Mazzoccoli G, Zoppi N, Grammatico P, Wade EM, Colombi M, Castori M, Micale L (2019) TAB2 c.1398dup variant leads to haploinsufficiency and impairs extracellular matrix homeostasis. *Hum Mutat* 40(10):1886-98. doi: 10.1002/humu.23834.

Mundlos S, Horn D (2014) Cooks syndrome. In: *Limb Malformations*. Springer-Verlag: Berlin Heidelberg, 101.

Palumbo O, Fichera M, Palumbo P, Rizzo R, Mazzolla E, Cocuzza DM, Carella M, Mattina T (2014) TBR1 is the candidate gene for intellectual disability in patients with a 2q24.2 interstitial deletion. *Am J Med Genet A* 164A(3):828-33. doi: 10.1002/ajmg.a.36363.

Palumbo O, Palumbo P, Di Muro E, Cinque L, Petracca A, Carella M, Castori M (2020) A Private 16q24.2q24.3 Microduplication in a Boy with Intellectual Disability, Speech Delay and Mild Dysmorphic Features. *Genes (Basel)* 11(6):707. doi: 10.3390/genes11060707.

Rao SS, Huntley MH, Durand NC, Stamenova EK, Bochkov ID, Robinson JT, Sanborn AL, Machol I, Omer AD, Lander ES, Aiden EL (2014) A 3D map of the human genome at kilobase resolution reveals principles of chromatin looping. *Cell* 159(7):1665-80. doi: 10.1016/j.cell.2014.11.021.

Riggs ER, Andersen EF, Cherry AM, Kantarci S, Kearney H, Patel A, Raca G, Ritter DI, South ST, Thorland EC, Pineda-Alvarez D, Aradhya S, Martin CL (2020) Technical standards for the interpretation and reporting of constitutional copy-number variants: A joint consensus recommendation of the American College of Medical Genetics and Genomics (ACMG) and the Clinical Genome Resource (ClinGen). *Genet Med* 22(2):245-257. doi: 10.1038/s41436-019-0686-8.

Rozen S, Skaletsky H (2000) Primer3 on the WWW for general users and for biologist programmers. *Methods Mol Biol* 132:365-86. doi: 10.1385/1-59259-192-2:365.

Silva M, de Leeuw N, Mann K, Schuring-Blom H, Morgan S, Giardino D, Rack K, Hastings R (2019) European guidelines for constitutional cytogenomic analysis. *Eur J Hum Genet* 27:1-16. doi: 10.1038/s41431-018-0244-x.

Spielmann M, Mundlos S (2013) Structural variations, the regulatory landscape of the genome and their alteration in human disease. *Bioessays* 35(6):533-43. doi: 10.1002/bies.201200178.

Legends to Figures

Figure 1

A-D Clinical features. **A:** left hand showing anonychia on fingers II-V, bulbous ends and shortened finger V. **B:** left foot with anonychia and shortening of the corresponding toes II-V. **C:** standard X-rays exam with missing phalanx on finger V and hypoplastic unguis tufts. Note partial dorsal duplication of the unguis tuft on finger II (magnification). **D:** standard X-rays exam showing toes II-V lacking a phalanx and with distal elongation and hypoplastic unguis tufts. **E** Partial karyotype showing translocation involving chromosome 1 and chromosome 17. **F-L** Fluorescence in situ hybridization (FISH) pattern on metaphase chromosomes. **F** Probe RP11-633A13 (g) (hg38 coordinates: chr17: 69873280...70055601), which maps upstream *KCNJ2*, shows two green signals at 17q24.3 identifying the normal and the translocated 17 chromosomes. **G** Probe N069H11 (o) (hg38 coordinates: chr17: 70039312...70241358), which maps at the *KCNJ2* locus, splits on both the chromosome 1 and 17 involved in translocation. **H** Probe RP11-727K24 (o) (hg38 coordinates: chr17: 71995502...72181723), which maps at the *SOX9* locus, shows two signals at the normal chromosome 17 and translocated chromosome 1. **I** Probes RP11-147B11 (g) (hg38 coordinates: chr1: 56452486...56617616) and RP-123K23 (o) (hg38 coordinates: chr1: 56856304...57040460), both mapping at 1p32.2 cytoband, show two signals at the normal chromosome 1 and translocated chromosome 17. **L** Probe RP11-706N07 (g) (hg38 coordinates: chr1: 60149164... 60365679), which maps at 1p32.1 cytoband, splits on both chromosomes 1 and 17 involved in the translocation. White dots indicate the chromosomal position of *KCNJ16*, *KCNJ2* and *SOX9*. g: green. o: orange.

Figure 2

A Results of SNP-Array analysis in the patient and her parents. Copy number state of each probe is drawn along chromosome band 17q24.3 (UCSC Genome Browser, build GRCh38/hg38). The upper panel represents the copy number state of the proband, her mother and father. Values of Y-axis indicate the inferred copy number according the probes intensities. Red bar indicates the deletion identified in the patient located between the genes *KCNJ16* and *KCNJ2*. The middle panel shows Hi-C map of the genomic region including the genes surrounding the structural variants while the lower panel represents previously published cases with Cooks syndrome and duplications (blue bars) at the 17q24.3 chromosome region (Kurth et al., 2009; Melo et al., 2020; Liu et al., 2020). Exemplificative cases of Pierre-Robin sequence and campomelic dysplasia with deletions at the same region (red bars) are from Kurth et al. (2009). **B** Breakpoint mapping of the germline t(1;17)(p32.1;q24.3) translocation. Whole-genome sequencing identified the potential breakpoints on the derivative chromosomes. Sanger sequencing of the resulting PCR products amplifying both breakpoint regions demonstrated the exact breakpoints on both derivative chromosomes. Sequence of chromosome 17 are in orange, sequence of chromosome 1 are in violet, microhomology is in red. Chromosomal positions are expressed in hg38. **C** Graphic representation of the chromosome 17. Genes of interest are depicted in blue, while the breakpoint generated by the *de novo* rearrangement is indicated in red.

Figure 3

A *In situ* Hi-C data of the *KCNJ2-SOX9* locus in IMR90 (chr17:67700000-72700000, hg38). The black arrow indicates the position of the translocation breakpoint. Gene annotation and putative enhancers from the ENCODE Encyclopedia are reported below (orange bars). Bar plots show normalized promoter capture Hi-C data from *KCNJ2* and *SOX9* promoters as point of view. **B** *In situ* Hi-C data of the genomic region around the breakpoint on chromosome 1 in IMR90 (chr1:57900000-62900000, hg38). Gene annotation and putative enhancers from the ENCODE Encyclopedia are reported below (orange bars). **C-E** qPCR analysis of endogenous *KCNJ2* and *SOX9* transcript level in patients' and controls' lymphocytes (C) and fibroblasts (D-E). The graphs show data from two independent experiments. Each point is averaged over three technical replicates.

*** p<0.01.

Figure S1

Results of SNP-Array analysis in the patient and her parents for the 1p32.1 locus. Copy number state and Log2ratio value of each probe is drawn along chromosome band 1p32.1 (UCSC Genome Browser, build GRCh38/hg38). The upper panel (green) represents the genomic profile of the proband, the middle panel (orange) that of the mother and the lower panel (blue) that of the father. Values of Y-axis indicate the inferred copy number according the probes intensities. Arrows indicate the 1p32.1 chromosomal region deleted in the patient, covered by 7 SNP array probes (C-4LHXN, C-7JZTB, S-4JLOO, S-4QMGC, S-3EEPD, C-5MLLL, C-5CRVZ).

Figure S2

qPCR analysis of endogenous *KCNJ16*, *SLC39A11*, *FGGY*, *DOCK7*, and *TAB2* transcript levels in patients' and controls' lymphocytes and fibroblasts. The graphs show data from two independent experiments. Each point is averaged over three technical replicates.

Figure 1

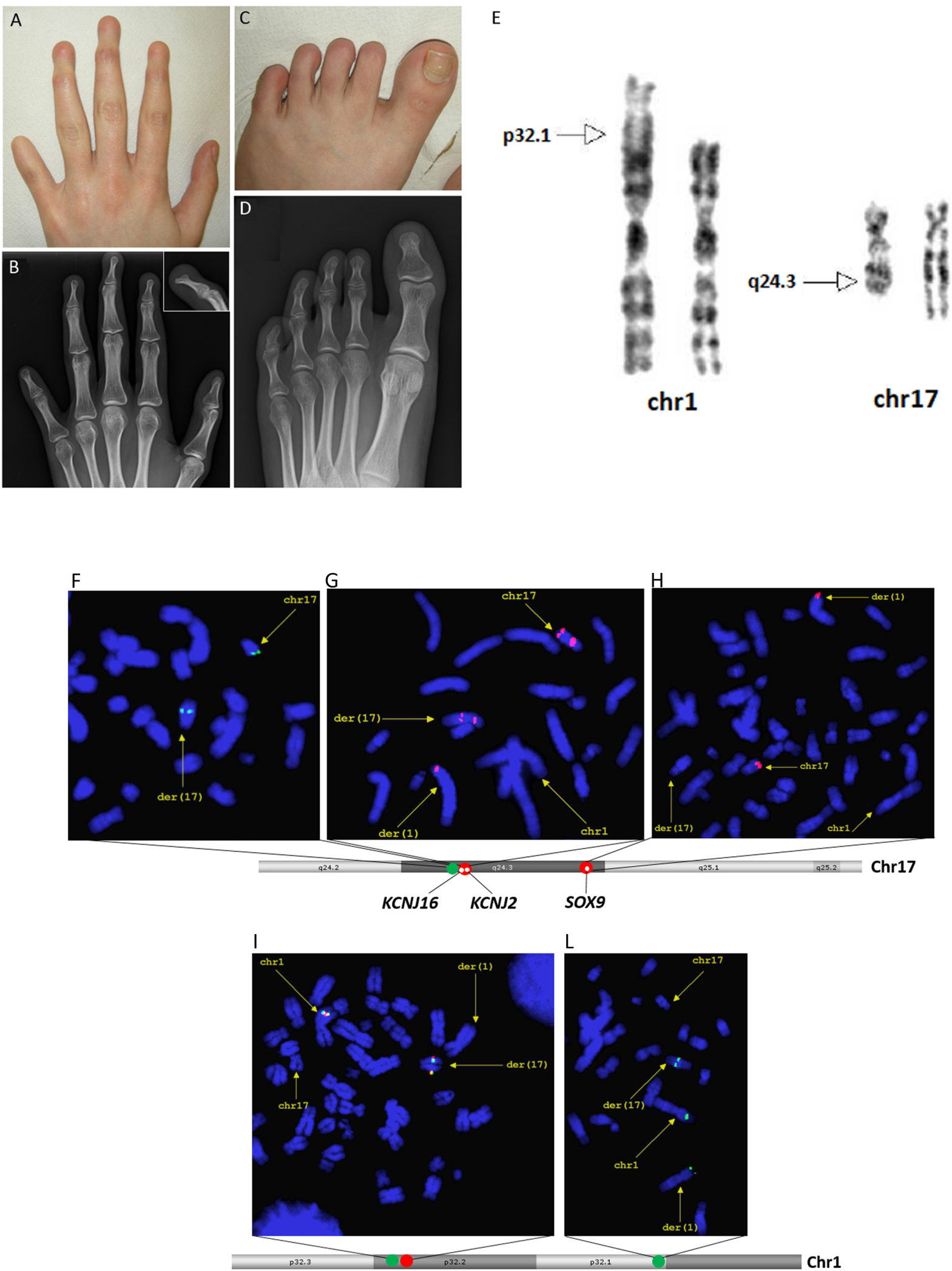
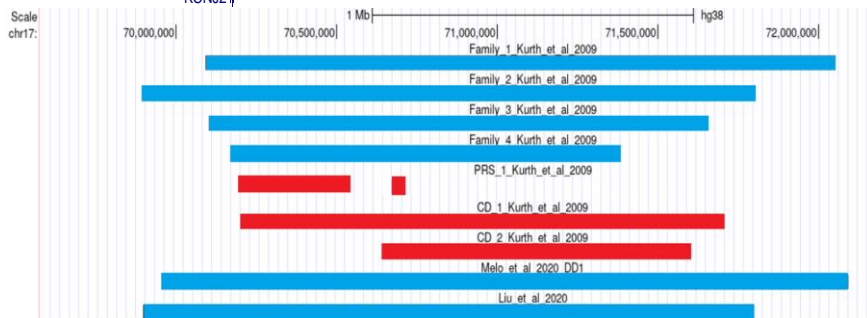
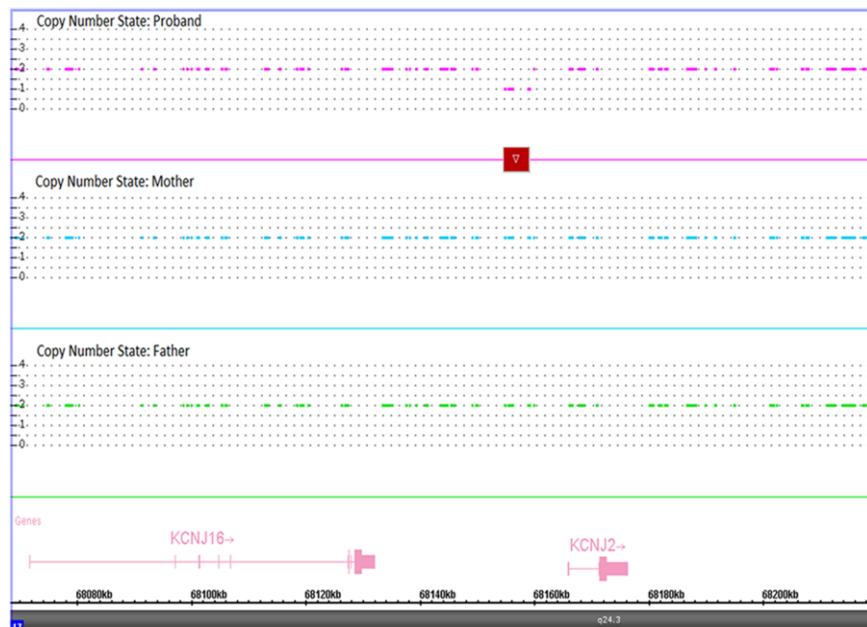
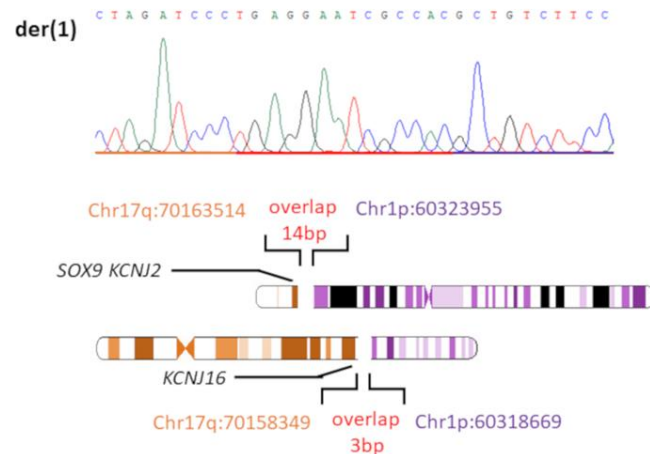


Figure 2

A



B



C

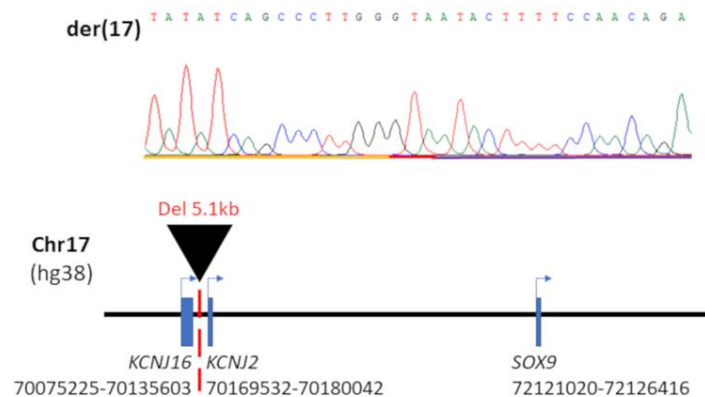


Figure 3

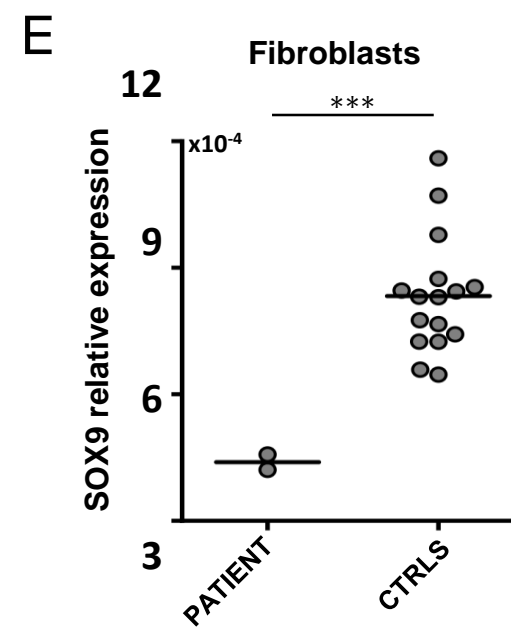
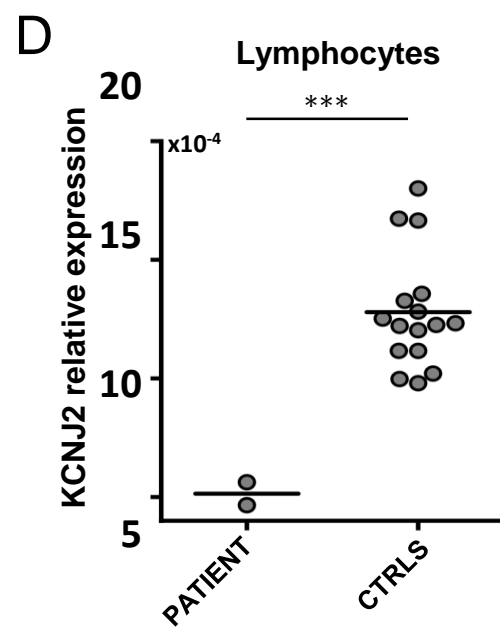
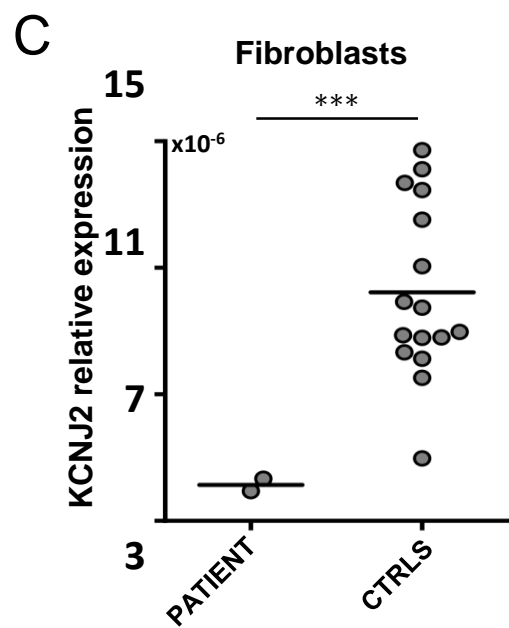
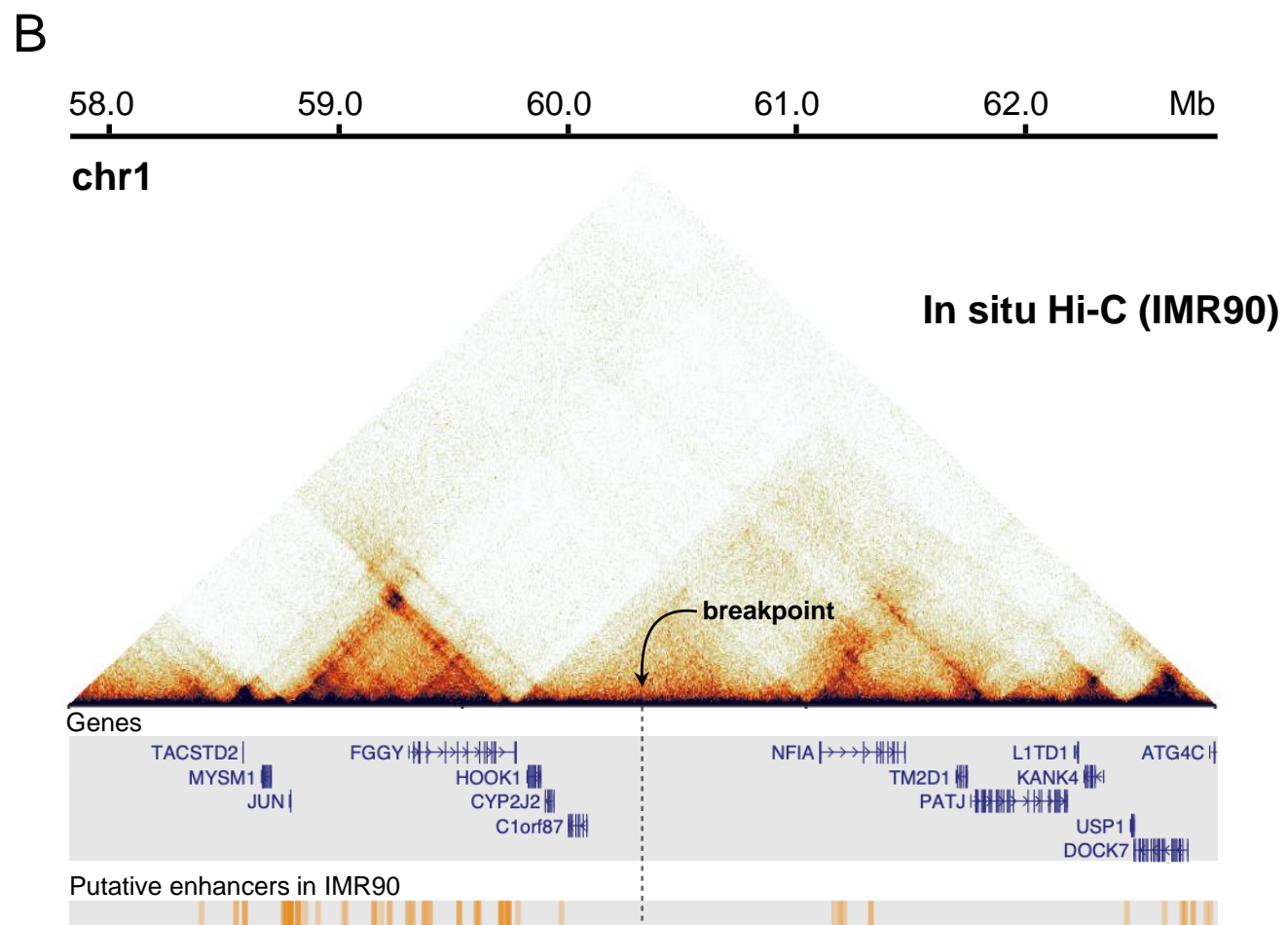
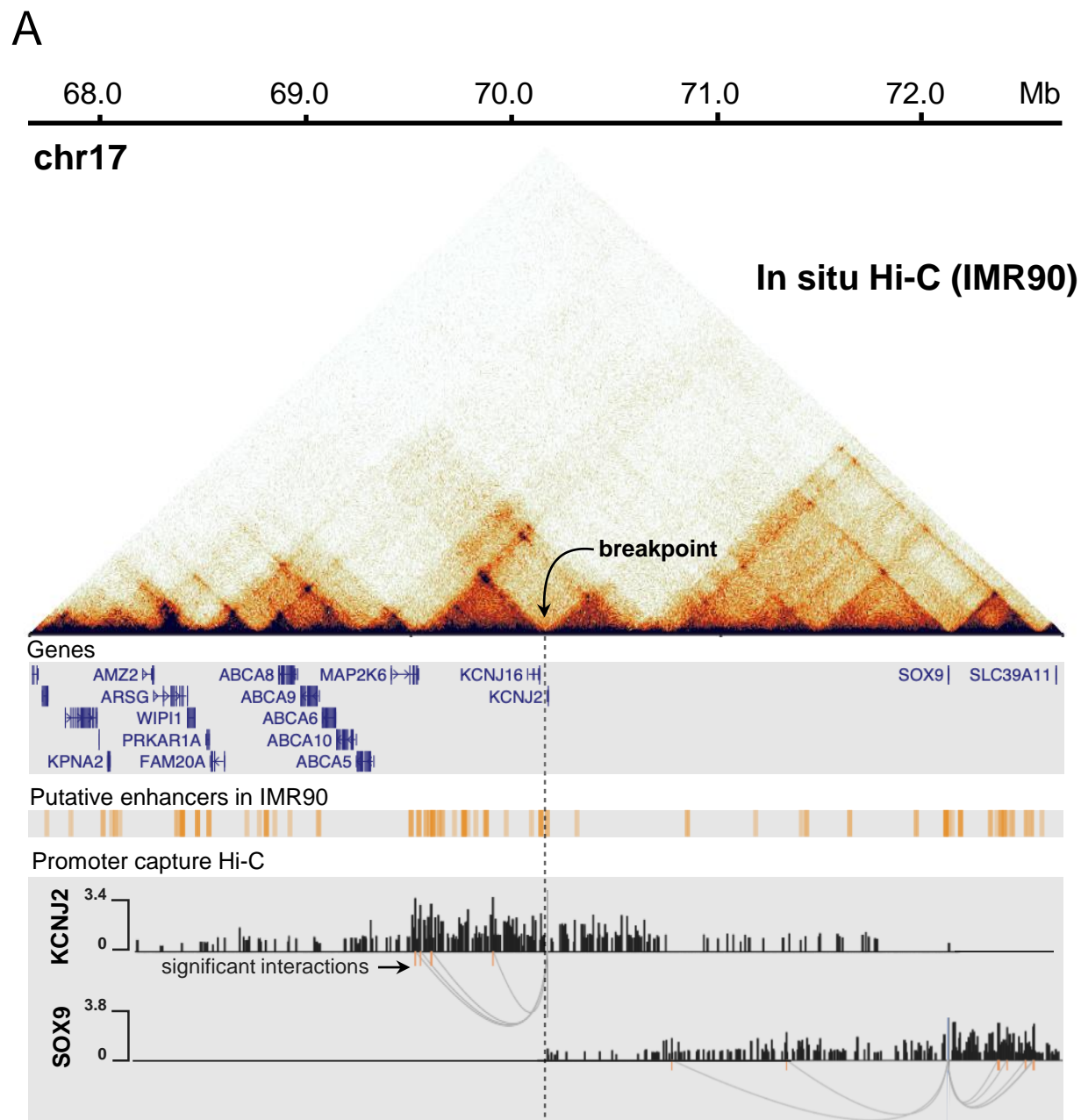
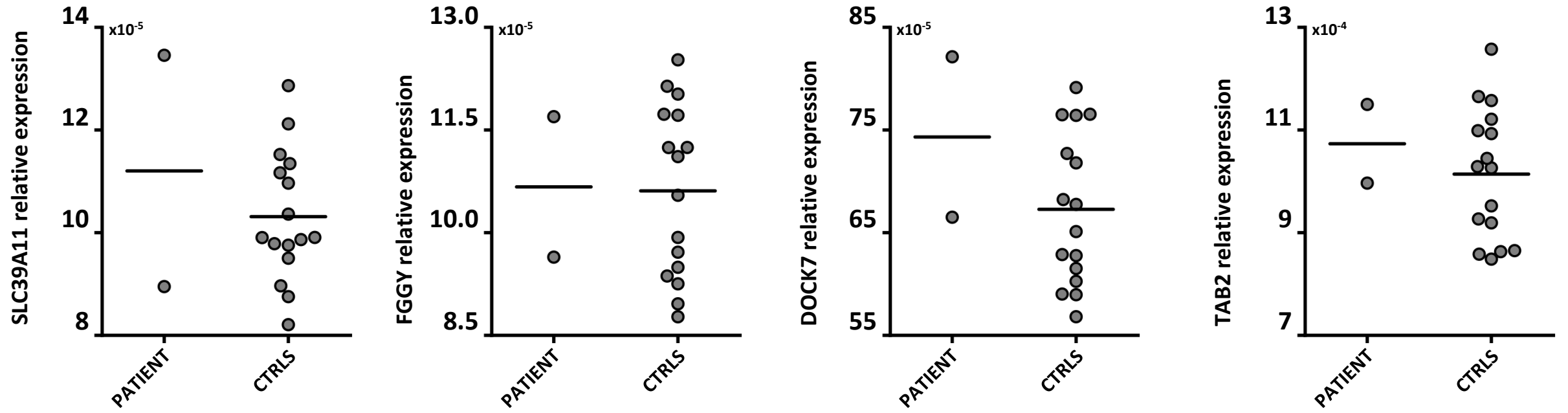


Figure S1



Figure S2

Fibroblasts



Lymphocytes

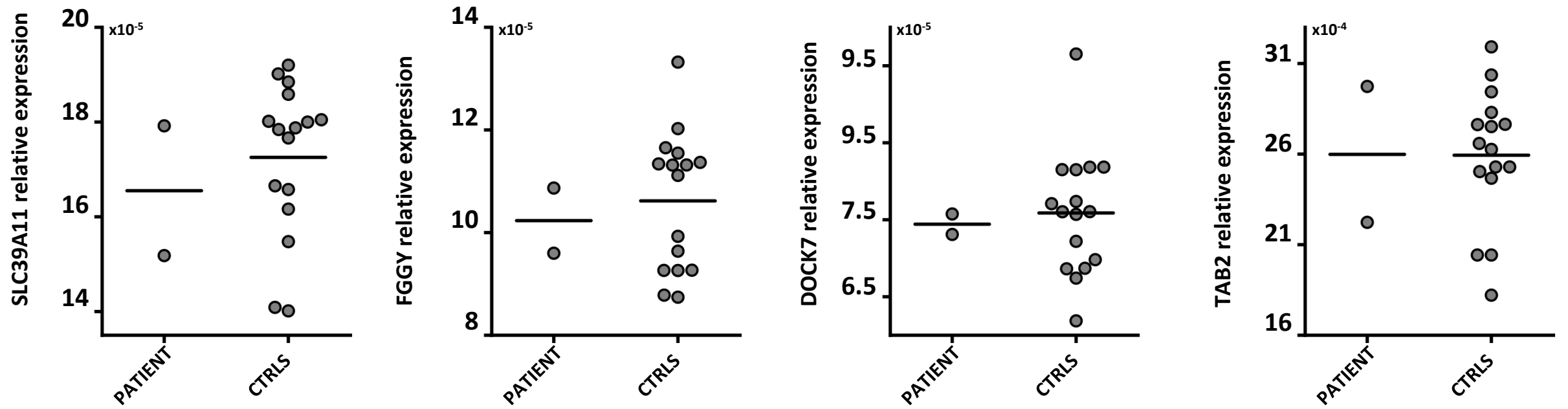


Table S1. Sequences of human primers used in this study.

Name	Sequence (5'-3')	Use
Breakpoint A-F	TTCAATCCCGATCCATAGTATCTGA	Sanger sequencing to confirm GS
Breakpoint A-R	ACTCACCGGCAAGTACATCT	Sanger sequencing to confirm GS
Breakpoint B-F	CGCCCGGCTGTAATGATAC	Sanger sequencing to confirm GS
Breakpoint B-R	TGGGCAAAGACTTCACGACT	Sanger sequencing to confirm GS
KCNJ2-ex2-F	CATCCAAAGAGGGCAAAGCT	Gene expression analysis
KCNJ2-ex2-R	GAGGAAGGCAGCCGTGAAG	Gene expression analysis
SOX9-ex3-F	AGCGACGTCATCTCCAACATC	Gene expression analysis
SOX9-ex3-R	GCGGCAGGTACTGGTCAAAC	Gene expression analysis
SLC39A11-ex2-3-F	TCTGTGTTCCAGGCCTTGCT	Gene expression analysis
SLC39A11-ex2-3-R	CCGCCTCTGTCCACTAGAGAA	Gene expression analysis
DOCK7-ex3-4-F	TCGGGACTGCAGAACTCTTGT	Gene expression analysis
DOCK7-ex3-4-R	TCTCTAACATGTGGATCCATTTAC	Gene expression analysis
FGGY-ex3-4-F	GCCACGTGTTCTCTGGTTGTT	Gene expression analysis
FGGY-ex3-4-R	CCCCTTCCTGGTTGACTGGTA	Gene expression analysis
TAB2-ex4-F	AGGCGCCTGAAAAGATCAAA	Gene expression analysis
TAB2-ex4-R	TCAGCTGCTGCATTTCTTCAA	Gene expression analysis
GAPDH-ex4-F	AATCCCATCACCATCTTCCA	Gene expression analysis
GAPDH-ex4-R	AAATGAGCCCCAGCCTTC	Gene expression analysis

GS: genome sequencing

Table S2. Rearrangement events identified by Genome Sequencing

Derivative	Chromosome	Position (t)	Reference sequence	Alternative sequence (p)
der(1)	17	70163500	G	[1:60323955[G
	1	60323941	T	[17:70163514[T
der(17)	1	60318669	T	T]17:70158352]
	17	70158349	G	G]1:60318672]

Genome Sequencing identified rearrangement events which are summarized in the table as a set of novel adjacencies. Each adjacency ties together 2 breakends. Meaning: t[p[sequence extending to the right of p is joined after t; t]p] reverse complement sequence extending left of p is joined after t.